# Isothermal and anisothermal implementations of 2D shape memory alloy modeling for transient impact response calculation

**Manuel COLLET**

FEMTO-ST Applied Mechanics - 24, chemin de l'épitaphe - 25000 Besançon - FRANCE

E-mail: manuel.collet@univ-fcomte.fr

**Morvan OUISSE**

E-mail: morvan.ouisse@univ-fcomte.fr

**Emmanuel FOLTÊTE**

E-mail: emmanuel.foltete@univ-fcomte.fr

**Christian LEXCELLENT**

E-mail: christian.lexcellent@univ-fcomte.fr

**Abstract.** A numerical implementation of the Raniecky Lexcellent (RL) [1, 2, 3] model for shape memory alloys (SMA) coupled with heat equation is presented in the paper, adapted to high strain rate loading. The objective is to predict the time response of a 2D SMA structure subjected to an impulse force and induced free vibration with a decreasing amplitude for isothermal and anisothermal conditions. The choice of the material mechanical properties has been done in order to have phases transformations during the oscillations. The apparent damping and stiffness effects due to these phase changes is clearly identified when the results are compared with a linear model without induced martensite. The thermomechanical constitutive relation of the SMA has been fullfiled to be able to take into account time reaction when the strain rate is very high. The full model has been implemented in a finite element code and tested on a 2D sample.

*Keywords*: Shape Memory Alloys, Non Linear Computation, Transient Impact Response

## 1. Introduction

Smart materials such as shape memory alloys (SMA) are used in different areas of engineering science. These materials, discovered around the 1930's are nowadays the source of unique and innovative applications. Using the framework of the beam theory, the one-dimensional structures (bars, springs...) can be designed empirically [4, 5]. In many cases, volumetric structures or plates, shells are made by using 3D or 2D models. A special numerical processing will be devoted to thin structures.

SMA modeling implies the introduction of the strongly nonlinear thermomechanical behavior associated with abrupt changes in their lattice structures called martensitic phase transformation [6]. Two common manifestations are: first, the shape memory effect corresponding to the reorientation of martensite platelets under external stress and second, the pseudoelasticity under stress associated to a recoverable phase transformation between a mother phase A called austenite and a product phase M called martensite.

The various applications of shape memory alloys have motivated a variety of constitutive models, see [7, 8] and the references therein.

When modeling these materials, the challenge is to find a balance between simplicity and adequate description of the underlying microstructure and its evolution.

Most of SMA models or solid-solid phase change ones lie within the framework of standard materials with internal variables [9].

It is well known that the macroscopic behavior of such materials can be described with two potentials: a free energy potential (Helmholtz or Gibbs) for the reversible aspects and a dissipation potential for the dissipative ones [10]. Moreover for these models, the choice of internal variables with physical meaning is important for physical characterization and updating processes. For instance, the choice of the volume fraction of martensite as an internal variable in a two-phases system is a natural one. Moreover the equations of conservation like the Euler-Cauchy equations of motion and energy related ones are needed if one wants to describe the dynamical behavior of such materials, because the Cauchy equation contains the acceleration, while the local temperature change is driven by the energy equation and its initial and boundary conditions, in a structure.

In the low range of temperature of use of SMA [-100°C, 150°C], the non linear SMA behavior is time independent (as it is the case for classical plasticity). The apparent time effect in SMA comes from the loading rate of the structure and the yield conditions. The behavior is always between isothermal for very low loading rate and adiabatic for very quick loading.

The problem of impact on a SMA device will tend near the second case.

In practical, impact can induce phase transformation. For instance, Escobar and Clifton [11] have conducted impact loading on a *Cu Al Ni* single crystal to induce a transformation from cubic austenite to monoclinic martensite. A thin plate was subjected to impact loading on one face with the resulting particle velocity measured

on the opposite face. In order to determine the kinetic law, Abeyaratne and Knowles [12, 13] have determined the driving force and the propagation speed of the phase boundary. Some experimental works related to damage behavior of shape memory alloy composites can be found in [14], and people are trying to integrate SMA-based devices in pre-crash systems or absorbing devices [15, 16]. The first approach is clearly fully experimental and the design is based on very simple considerations on the behavior of the SMA device. Nevertheless, precise models are required in order to be able to evaluate the ability of the designed devices to respond to all constraints in an industrial domain, and also to be able to perform some parametric studies in order to find the best compromise among the many available materials and designs. As far as the modeling dedicated to impact on SMA structures is concerned, no dedicated paper seems to have been published. One can note that some works on impact behavior exist [17], but no structural effect is considered. Including macroscopic SMA constitutive laws in finite elements (FE) models is clearly one of the most pertinent ways to exhibit physical behavior or SMA-based structures in the time domain. Several works on this topic can be found in the literature, among which the works presented in [18], [19], [20]. Among the models which are available for transient calculations, none of them has been explicitely applied in the context of structural response to impact including thermal effects. The specificity of the fast transient analysis of SMA-based structures is that the constitutive laws of the materials are highly non linear, which induces numerical troubles during time integration. In this paper, the Raniecky-Lexcellent *RL* model [1, 2, 3], which has already been successfully applied in a "low frequency" application [18], is extended and adapted to the case of structural response to impact.

## 2. Partial Differential Equations Defining the Shape Memory Alloy Dynamical Equilibrium

In order to present a complete and rigorous implementation of the mechanical behavior, let us start by considering the generic dynamical equilibrium of a structure made of Shape Memory Alloy material like illustrated in figure 1. The thermomechanical system covers the closed domain $\Omega$ with a boundary named $\Gamma = \Gamma_u \cup \Gamma_t = \Gamma_q \cup \Gamma_T$ where the boundary partition surfaces are $\Gamma_u$, $\Gamma_t$, $\Gamma_q$ and $\Gamma_T$, associated to borders on which displacement $\mathbf{U_0}$, force $\mathbf{F_0}$, thermal flux $q_0$ and temperature $T_0$ are respectively imposed. The thermomechanical forces applied inside the domain include mechanical and thermal loads, respectively called $\mathbf{f_m}$ and $f_T$. $\mathbf{U}$ represents the unknown vector of displacements and $T$ the unknown temperature. In figure 1, $\mathbf{n}$ stands for the outpointing normal vector.

Unless indicated, all physical variables are functions of space ($\mathbf{M}$ is the generic point) and time $t$, and all parameters are constant. The time interval of interest is denoted by $\mathcal{T}$.

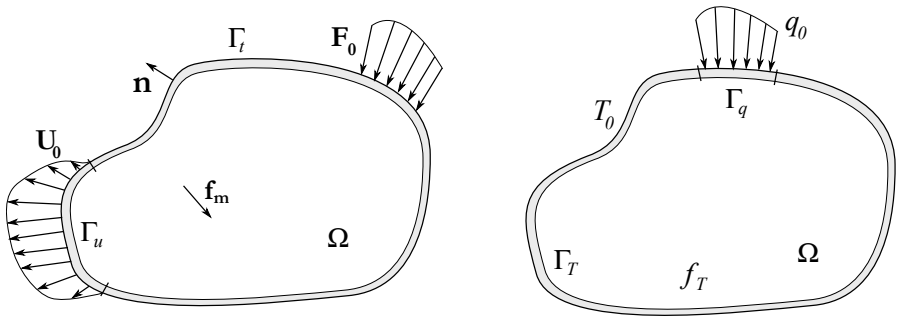


**Figure 1.** Thermodynamic problem - mechanical and thermal domain description and boundary conditions

### *2.1. Statement of thermomechanical dynamical problem*

Under the assumptions of small strain and displacements, the thermomechanical dynamical problem satisfies the following fundamental equations:

- The mechanical dynamical equilibrium

$$\rho\ddot{\mathbf{U}} - \boldsymbol{\nabla}\cdot\boldsymbol{\sigma} = \mathbf{f_m} \quad \forall(\mathbf{M},t) \in \Omega\times\mathcal{T}, \tag{1}$$

  where $\rho$ represents the material density and $\boldsymbol{\sigma}$ the Cauchy stress tensor.

- The first thermodynamic principle (energy conservation)

$$\rho\dot{u} - \boldsymbol{\nabla}\cdot\mathbf{q} = \boldsymbol{\sigma} : \dot{\boldsymbol{\varepsilon}} + f_T \quad \forall(\mathbf{M},t) \in \Omega\times\mathcal{T}, \tag{2}$$

  where $u$ is the total energy, $\mathbf{q}$ the vector of thermal flux and $\boldsymbol{\varepsilon}$ the Green-Lagrange strain tensor:

$$\boldsymbol{\varepsilon} = \frac{1}{2}(\boldsymbol{\nabla}\cdot\mathbf{U}^T + \mathbf{U}\cdot\boldsymbol{\nabla}^T), \tag{3}$$

  which is dual to the Cauchy stress tensor $\boldsymbol{\sigma}$. The constitutive equations will be given in section 2.3.

- The second thermodynamic principle

$$\rho T\dot{s} - \rho f_T + \boldsymbol{\nabla}\cdot\mathbf{q} - \frac{1}{T}\mathbf{q}\cdot\boldsymbol{\nabla}T \geq 0 \quad \forall(\mathbf{M},t) \in \Omega\times\mathcal{T}, \tag{4}$$

  where $s$ represents the specific entropy of the material.

  The boundary conditions on $\Gamma_u$, $\Gamma_t$, $\Gamma_q$ and $\Gamma_T$ can be written:

$$\begin{cases} \mathbf{U} = \mathbf{U_0} & \forall(\mathbf{M},t) \in \Gamma_u\times\mathcal{T}, \\ \boldsymbol{\sigma}\cdot\mathbf{n} = \mathbf{F_0} & \forall(\mathbf{M},t) \in \Gamma_t\times\mathcal{T}, \\ T = T_0 & \forall(\mathbf{M},t) \in \Gamma_T\times\mathcal{T}, \\ \mathbf{q}\cdot\mathbf{n} = q_0 & \forall(\mathbf{M},t) \in \Gamma_q\times\mathcal{T}. \end{cases} \tag{5}$$

  Finally, the problem is closed by the initial conditions at $t = t_0$:

$$\begin{cases} \mathbf{U}(\mathbf{M},t_0) = \mathbf{U_i}(\mathbf{M}) & \forall\mathbf{M} \in \Omega, \\ \dot{\mathbf{U}}(\mathbf{M},t_0) = \mathbf{V_i}(\mathbf{M}) & \forall\mathbf{M} \in \Omega, \\ T(\mathbf{M},t_0) = T_i(\mathbf{M}) & \forall\mathbf{M} \in \Omega. \end{cases} \tag{6}$$

### *2.2. Shape Memory Alloys behavior*

The behavior considered in this paper is related to phase change of SMAs. At stress free state and $T = T_i$, the material is supposed to be fully austenitic (A). During the load, the phase can change locally for martensite. A macromodel of the behavior considers a two-phase reference elementary volume containing the volume fraction $(1-\xi)$ of mother phase (Austenite A) and $\xi$ of product phase (Martensite M).

A typical stress-strain curve is given in figure 2. Let us suppose that, at a given temperature, one performs an increasing and decreasing strain load. The SMA will typically describe a loop in the stress-strain plane:

(i) Load increase: while the stress-strain point is below a given limit described by the line $\pi^f = 0$ that will be detailed in the next section, the behavior is linear elastic and the material is fully austenitic ($\xi = 0$).

(ii) Load increase: when the stress-strain point reaches the $\pi^f = 0$ line, the phase transformation begins ($\xi$ increases in $[0, 1]$). The rigidity of the material is affected by the phase transformation, which can go theoretically up to the full martensite state ($\xi = 1$), in which case the behavior is becoming linear again.

(iii) Load decrease: while the stress-strain point stays above the $\pi^f = 0$ line, the behavior is linear elastic and $\xi$ remains constant.

(iv) Load decrease: when the stress-strain point reaches the $\pi^f = 0$ line, the reverse phase transformation occurs ($\xi$ decreases in $[0, 1]$). The rigidity of the material is affected by the phase transformation, which can go down to the full austenite state ($\xi = 0$).

The behavior described on figure 2 corresponds to a 'classical' and 'simple' representation of such phenomenon. We underline that such loading/unloading curve is only one among others possible behavior obtained by coupling thermally induced and stress-induced transformation as presented in Airoldi and al [21] or by considering tension/compression asymmetry as in Raniecky [2]. This kind of behavior is not yet included in the following methodology even if tension/compression asymmetry, for example, could be easily added to the proposed numerical implementation.

One also knows that material properties of Austenite and Martensite can be very different for certain SMA. In this work, we only focused our analysis on numerical implementation of dynamic response of mostly austenitic SMA. The 'Martensitic' part of the structural behavior is also considered as residual compared to what happens during the phase transformation. So, in this paper, no difference between mechanical properties of each SMA phases neither reorientation between martensitic variants is taken into consideration. Some specific modifications of the proposed numerical implementation could allow introduction of such specific phase mechanical behavior.

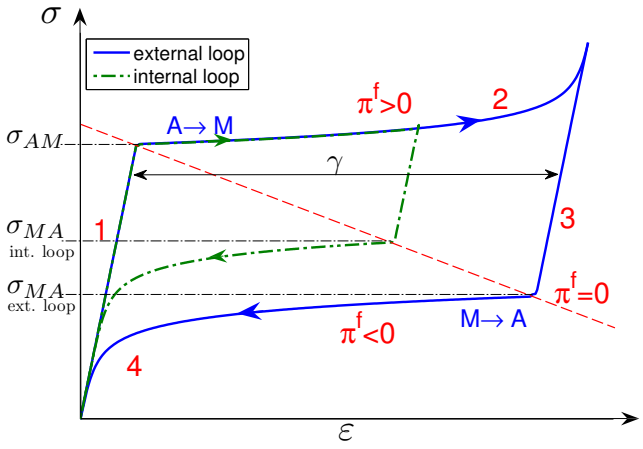


**Figure 2.** Typical SMA behavior: 1D stress-strain evolution including internal (partial transformation) and external (full transformation) loops

### *2.3. Material thermo-mechanical constitutive equations: the RL model for shape memory alloys*

Whatever the considered material, its thermodynamic states obey to fundamental equations of conservation (1), (2), (4). By using the theory of the thermodynamics of irreversible processes and thermodynamic potential functions, the constitutive behavior equations can be obtained through the expression of Helmholtz free energy $\phi$ such as:

$$\phi = u - Ts. \tag{7}$$

Thus one has $\mathfrak{o} = \rho\dfrac{\partial\phi}{\partial\mathfrak{e}}$ and $s = -\dfrac{\partial\phi}{\partial T}$. When new internal variables are introduced, the same kind of relations provide constitutive equation for each pair of dual states.
The SMA description which has been implemented is based on the *RL* model [1], built by using this kind of approach. In this paper, isothermal and anisothermal transformations have been considered in a fully multiphysics approach in order to test the ability of the model to respond to structural impacts with various thermal conditions.

In this way, the Helmholtz free energy is defined for the two-phase reference volume element (RVE) containing the volume fraction $(1-\xi)$ of mother phase (Austenite A) and $\xi$ of product phase (Martensite M) as:

$$\begin{aligned}\phi(\mathfrak{e},\xi,T) = \; & u_0^{(A)} - Ts_0^{(A)} - \xi\pi_0^f(T) + \tfrac{1}{2}\left(\mathfrak{e}-\mathfrak{e}^{tr}-\mathfrak{e}^{th}\right):\mathbb{L}:\left(\mathfrak{e}-\mathfrak{e}^{tr}-\mathfrak{e}^{th}\right) \\ & +\xi(1-\xi)\phi_{it} + C_v\left(T - T_0 - T\cdot\ln\tfrac{T}{T_0}\right),\end{aligned} \tag{8}$$

where:

- $u_0^{(A)}$ (resp. $u_0^{(M)}$) is the internal energy of austenite (resp. martensite) phase,
- $s_0^{(A)}$ (resp. $s_0^{(M)}$) is the internal entropy of austenite (resp. martensite) phase,
- $\pi_0^f(T)$ is the driving force at free stress state defined as $\pi_0^f(T) = \Delta u_0 - T\Delta s_0$, with $\Delta u_0 = u_0^{(A)} - u_0^{(M)}$ and $\Delta s_0 = s_0^{(A)} - s_0^{(M)}$,

- $\mathbb{e}^{tr}$ is the phase transformation strain tensor,
- $\mathbb{e}^{th}$ is the thermal expansion strain tensor: $\mathbb{e}^{th} = (T-T_0)\alpha\mathbb{I}$, where $\alpha$ is the dilatation coefficient and $\mathbb{I}$ is the identity tensor of order 2,
- $\mathbb{L}$ is the fourth-order Hooke tensor,
- $\phi_{it}$ is a coefficient corresponding to internal interaction energy,
- $C_v\left(T - T_0 - T\cdot\ln\frac{T}{T_0}\right)$ is the specific heat energy, with $C_v$ corresponding to the specific heat coefficient at constant volume.

The Helmholtz free energy given in equation (8) leads to express the mechanical multiphysics constitutive equation as:

$$\mathbb{\sigma} = \mathbb{L} : \left(\mathbb{e} - \mathbb{e}^{tr} - (T - T_0)\alpha\mathbb{I}\right) = \mathbb{L} : \mathbb{e}^{e}. \tag{9}$$

The elastic strain tensor $\mathbb{e}^e = \mathbb{e} - \mathbb{e}^{tr} - (T-T_0)\alpha\mathbb{I}$ is also constituted of three terms: the mechanical Green strain tensor $\mathbb{e}$, the phase transformation induced strain $\mathbb{e}^{tr}$ and the thermal strain $(T - T_0)\alpha\mathbb{I}$.

The *RL* model gives the expression of $\mathbb{e}^{tr}$ such as:

$$\mathbb{e}^{tr} = \gamma\xi\mathbb{K} \text{ with } \mathbb{K} = \frac{3}{2}\frac{\mathbb{dev}\,(\mathbb{\sigma})}{\sigma_{vm}}, \tag{10}$$

in which $\gamma$ is the pure tension deformation associated to the phase transformation. This material parameter is indicated in figure 2. $\sigma_{vm}$ represents the Von Mises equivalent stress and $\mathbb{dev}\,(\mathbb{\sigma})$ the deviator stress tensor:

$$\begin{aligned} \sigma_{vm} &= \sqrt{\tfrac{3}{2}\mathbb{dev}\,(\mathbb{\sigma}) : \mathbb{dev}\,(\mathbb{\sigma})}, \\ \mathbb{dev}\,(\mathbb{\sigma}) &= \mathbb{\sigma} - \frac{\mathrm{tr}(\mathbb{\sigma})}{3}\mathbb{I}, \end{aligned} \tag{11}$$

where tr is the *trace* operator.

Incorporating expression (10) into equations (9) and (8), and defining a so-called driving force of phase transformation under mechanical loading $\pi^f$, which is linked to the Helmholtz free energy by the relationship $\pi^f(\sigma_{vm}, \xi, T) = -\rho\dfrac{\partial\phi}{\partial\xi}$, one obtains:

$$\pi^f(\sigma_{vm}, \xi, T) = \frac{\gamma\sigma_{vm}}{\rho} + \pi_0^f(T) - (1 - 2\xi)\phi_{it}(T). \tag{12}$$

The last step in the model formulation is to impose constitutive equations insuring the second thermodynamic principle. The corresponding inequality (4) can be rewritten using the Helmholtz free energy expression (7)

$$\mathbb{\sigma} : \dot{\mathbb{e}} - \rho\left(\dot{\phi} + s\dot{T}\right) - \frac{1}{T}\mathbf{q}\cdot\boldsymbol{\nabla}T \geq 0. \tag{13}$$

Inequality (13) exhibits two terms, the first one $D_{int} = \mathbb{\sigma} : \dot{\mathbb{e}} - \rho\left(\dot{\phi} + s\dot{T}\right)$ corresponds to intrinsic dissipation while $D_{th} = -\dfrac{1}{T}\mathbf{q}\cdot\boldsymbol{\nabla}T$ is associated to thermal

dissipation. It is assumed that each term is positive (i.e $D_{th} \geq 0$ and $D_{int} \geq 0$), which obviously implies a thermodynamic transformation satisfying the second principle (13).

Thus, one can assume a standard Fourier conduction behavior such as:

$$\mathbf{q} = -\lambda \boldsymbol{\nabla} T, \tag{14}$$

that easily verifies the condition $D_{th} \geq 0$.

By using the specific expression of SMA free energy given in equation (8), the second inequality constraint $D_{int} \geq 0$ becomes

$$\pi^f(\sigma_{vm}, \xi, T) \cdot \dot{\xi} \geq 0. \tag{15}$$

The phase transformation kinetics are written using the formal expression

$$\dot{\xi} = \mathcal{F}(\dot{\sigma}_{vm}, \pi_f, \xi) \text{ with } \xi \in [0, 1]. \tag{16}$$

According to the *RL* model, a state flow algebraic expression of function $\mathcal{F}$ depending on the thermodynamic state of the considered material point can be proposed by introducing some boolean conditions.

- For Austenite to Martensite transformation ($\xi \in ]0, 1[$ and $\dot{\sigma}_{vm} > 0$ and $\pi_f(T) > 0$), one has:

$$\mathcal{F}(\dot{\sigma}_{vm}, \pi_f, \xi) = \frac{\gamma \dot{\sigma}_{vm}}{\rho \left( \dfrac{A_1}{1-\xi} - 2\phi_{it} \right)}. \tag{17}$$

- For Martensite to Austenite transformation ($\xi \in [0, 1]$ and $\dot{\sigma}_{vm} \leq 0$ and $\pi_f(T) \leq 0$), one has:

$$\mathcal{F}(\dot{\sigma}_{vm}, \pi_f, \xi) = \frac{\gamma \dot{\sigma}_{vm}}{\rho \left( \dfrac{A_2}{\xi} - 2\phi_{it} \right)}. \tag{18}$$

- In other cases, in particular for the full austenite phase ($\xi = 0$) and the full martensite phase ($\xi = 1$), one has:

$$\mathcal{F}(\dot{\sigma}_{vm}, \pi_f, \xi) = 0. \tag{19}$$

These state flow kinetic relationships obviously satisfy the second inequality constraint $D_{int} \geq 0$. These expressions can be compactly written as:

$$\mathcal{F}(\dot{\sigma}_{vm}, \pi_f, \xi) = \frac{\gamma \dot{\sigma}_{vm}}{\rho} \left( \frac{H(\pi_f) H(\dot{\sigma}_{vm})}{\dfrac{A_1}{1-\xi} - 2\phi_{it}} + \frac{H(-\pi_f) H(-\dot{\sigma}_{vm})}{\dfrac{A_2}{\xi} - 2\phi_{it}} \right). \tag{20}$$

This function includes some no differential Heaviside distributions $H$ which would introduce numerical difficulties for Jacobian evaluation and for solving the associated non linear problem.

One can notice that the *RL* model can be written using explicit expressions of volume fraction of the martensite $\xi$ like indicated in [22], but these expressions are not convenient at a numerical point of view in the context of finite element, since in each

node of the mesh one has to remember the value of $\xi$ just before the last inversion of phase transformation. This is a difficult point, in particular in the context of structural dynamics, and using this kind of approach would induce numerical troubles. Using first-order time derivative equation like (16) helps regularizing the problem. One can also note that the constraint $\xi \in [0,1]$ is theoretically already included in kinetics equation (20), since explicit time integration results in bounded expression [22], but numerical time integration induces loss of $[0,1]$ bounds for variable $\xi$. For that reason, the constraint $0 \leq \xi \leq 1$ is included in the set of equations which is considered here.

### *2.4. Set of equations describing the behavior of the SMA structure*

The equilibrium equations can be rewritten by introducing constitutive equations allowing to guaranty the second thermodynamic principle. This leads to the following set of partial derivative equations driving the thermomechanical dynamical equilibrium of shape memory alloy structure as described in figure 1:

$$
\begin{array}{ll}
\rho\ddot{\mathbf{U}} - \boldsymbol{\nabla}\cdot\boldsymbol{\sigma} = \mathbf{f_m} & \forall(\mathbf{M},t) \in \Omega\times\mathcal{T}, \\
\rho C_v\dot{T} - \lambda\boldsymbol{\nabla}^2 T - f_T = & \\
\rho\left(\pi^f(\sigma_{vm},\xi,T) + T\Delta s_o - (1-\xi)\right)\dot{\xi} - \alpha T\mathrm{tr}(\dot{\boldsymbol{\sigma}}) & \forall(\mathbf{M},t) \in \Omega\times\mathcal{T}, \\
\boldsymbol{\sigma} = \mathbb{L} : (\boldsymbol{\varepsilon} - \gamma\xi\mathbb{K} - (T-T_0)\alpha\mathbb{I}) & \forall(\mathbf{M},t) \in \Omega\times\mathcal{T}, \\
\mathbb{K} = \dfrac{3}{2}\dfrac{\mathbb{dev}(\boldsymbol{\sigma})}{\sigma_{vm}} & \forall(\mathbf{M},t) \in \Omega\times\mathcal{T}, \\
\dot{\xi} = \mathcal{F}(\dot{\sigma}_{vm},\pi_f,\xi) & \forall(\mathbf{M},t) \in \Omega\times\mathcal{T}, \\
0 \leq \xi \leq 1 & \forall(\mathbf{M},t) \in \Omega\times\mathcal{T}, \\
\boldsymbol{\sigma}\cdot\mathbf{n} = \mathbf{F_0} & \forall(\mathbf{M},t) \in \Gamma_t\times\mathcal{T}, \\
\mathbf{U} = \mathbf{U_0} & \forall(\mathbf{M},t) \in \Gamma_u\times\mathcal{T}, \\
T = T_0 & \forall(\mathbf{M},t) \in \Gamma_T\times\mathcal{T}, \\
\mathbf{q}\cdot\mathbf{n} = h_0(T-T_0) & \forall(\mathbf{M},t) \in \Gamma_q\times\mathcal{T}, \\
\mathbf{U}(\mathbf{M},t_0) = \mathbf{U_i}(\mathbf{M}) & \forall\mathbf{M} \in \Omega, \\
\dot{\mathbf{U}}(\mathbf{M},t_0) = \mathbf{V_i}(\mathbf{M}) & \forall\mathbf{M} \in \Omega, \\
T(\mathbf{M},t_0) = T_i(\mathbf{M}) & \forall\mathbf{M} \in \Omega.
\end{array}
\tag{21}
$$

### *2.5. Numerical issues*

The mathematical problem (21) is strongly non linear and presents specific numerical difficulties which need to be solved:

(i) The constraint $\boldsymbol{\sigma}$ given by the third equality of problem (21) exhibits a numerical algebraic loop because of the direct non linear dependency of $\mathbb{K}$ tensor in $\boldsymbol{\sigma}$ expression. This algebraic loop can not be solved explicitly because the expression of tensor $\mathbb{K}$ given in equation (10) (i.e $\mathbb{K} = \dfrac{3}{2}\dfrac{\mathbb{dev}(\boldsymbol{\sigma})}{\sigma_{vm}}$) appears as a strongly irregular non linear tensorial function. Indeed, this function, looking for $\frac{\mathbb{x}}{\|\mathbb{x}\|}$ on tensorial space, presents a singularity when $\mathbb{x} = \mathbb{O}$. As the dynamical simulation aims at

exhibiting vibrating movements, a regularization should be introduced to efficiently solve the problem.

(ii) The second difficulty lies in the state flow differential equation giving kinetics of martensite volume fraction variable $\xi$ in the fifth equation of system (21), constrained by inequalities $0 \leq \xi \leq 1$. The state flow differential equation contains irregular Heaviside distribution functions that can not be directly introduced in non linear solver using Jacobian matrix evaluation in a Newton-Raphson algorithm, these distributions being underivable.

One of the key point of this work is to propose a specific mathematical processing to deal with each particular underlining numerical problems.

*2.5.1. Treatment of the numerical algebraic loop* The algebraic loop, i.e $\mathfrak{o} = \mathbb{L} : \left(\mathfrak{e} - \gamma\xi\mathbb{K}_{(\mathbf{M},t)} - (T - T_0)\alpha\mathbb{I}\right)$, can be regarded as one time step ahead response. From a physical point of view, this no casual operator should be translated into a step time casual relationship $\mathfrak{o} = \mathbb{L} : \left(\mathfrak{e} - \gamma\xi\mathbb{K}_{(\mathbf{M},t-dt)} - (T - T_0)\alpha\mathbb{I}\right)$. Thus the stress tensor is not depending on its value at the considered time but only at the previously evaluated time. The idea is then to evaluate $\mathbb{K}$ as a solution of an ordinary differential equation in time by introducing a specific time delay using a corresponding parameter $t_k$ instead of the direct relationship given by equation (10) such as:

$$\frac{3}{2}\mathbb{dev}(\mathfrak{o}) - \left(\mathbb{K} + t_k.\dot{\mathbb{K}}\right)(\sigma_{vm} + \alpha) = 0 \quad \forall(\mathbf{M}, t) \in \Omega \times \mathcal{T}. \tag{22}$$

*2.5.2. Implementation of the state flow equations constrained by inequalities* The inequality constraints (i.e $0 \leq \xi \leq 1$) can be transformed by using existence of two new functions $\beta_1$ and $\beta_2$ so that $\beta_1^2 + \beta_2^2 = 1$ and $\xi = \dfrac{\beta_1^2 - \beta_2^2 + 1}{2}$. It can be can easily demonstrated that $\xi \geq 0$ is equivalent to the existence of a real variable $\beta_1$ such as $\xi = \beta_1^2$, while $\xi \leq 1$ is equivalent to the existence of a real variable $\beta_2$ such as $1 - \xi = \beta_2^2$. A change of variable $\xi = \dfrac{\beta_1^2 - \beta_2^2 + 1}{2}$ in equations of system (21) is operated and a new constraint $\beta_1^2 + \beta_2^2 = 1$ is added to this set of equations.

The irregular state flow operators (i.e the Heaviside distribution functions) are regularized by using dedicated function $\tilde{H}(x, \delta)$ corresponding to smoothed Heaviside function in the interval $-\delta < x < \delta$ with a continuous second derivative without overshoot. It is defined by a sixth-degree polynomial expression ($flc2hs$ function in Comsol Multiphysics software). The nonlinear function $\mathcal{F}(\dot{\sigma}_{vm}, \pi_f, \xi)$ defined in (20) is then rewritten:

$$\tilde{\mathcal{F}}(\dot{\sigma}_{vm}, \pi_f, \beta_1, \beta_2) = \frac{\gamma\dot{\sigma}_{vm}}{\rho}\left(\frac{\tilde{H}(\pi_f - \delta_1, \delta_1)\cdot\tilde{H}(\dot{\sigma}_{vm} - \delta_2, \delta_2)}{\dfrac{A_1}{1 - \frac{\beta_1^2 - \beta_2^2 + 1}{2}} - 2\phi_{it}}\right.$$

$$+\frac{\tilde{H}(-\pi_f-\delta_1,\delta_1)\cdot\tilde{H}(-\dot{\sigma}_{vm}-\delta_2,\delta_2)}{\frac{A_2}{\frac{\beta_1^2-\beta_2^2+1}{2}}-2\phi_{it}}\Bigg). \quad (23)$$

In the numerical simulations, $\delta_1 = 200$ and $\delta_2 = 10$ have been used. The phase transformation kinetic equation (16) is finally rewritten by incorporating the new variables $\beta_1$ and $\beta_2$ and adding time regularization using time delay parameter $t_m$. This time parameter can be chosen depending on the speed of sound in the alloy. The new kinetic equation is:

$$t_m\ddot{\beta_1}-(\beta_1\dot{\beta_1}-\beta_2\dot{\beta_2})\cdot\tilde{\mathcal{F}}(\dot{\sigma}_{vm},\pi^f,\beta_1,\beta_2)=0. \quad (24)$$

*2.5.3. Regularized set of partial derivative equations modeling the Shape Memory Alloy thermo-mechanical equilibrium* The set of equations (21) can be rewritten by introducing the proposed changes. The final system of partial derivative equations modeling the SMA thermo-mechanical equilibrium is:

$$\begin{array}{ll}
\rho\ddot{\mathbf{U}}-\boldsymbol{\nabla}\cdot\boldsymbol{\sigma}=\mathbf{f_m} & \forall(\mathbf{M},t)\in\Omega\times\mathcal{T},\\
\rho C_v\dot{T}-\lambda\boldsymbol{\nabla}^2T-f_T= & \\
\rho\left(\pi^f(\sigma_{vm},\xi,T)+T\Delta s_o-(1-\xi)\right)\dot{\xi}-\alpha T\mathrm{tr}(\dot{\boldsymbol{\varepsilon}}) & \forall(\mathbf{M},t)\in\Omega\times\mathcal{T},\\
\boldsymbol{\sigma}=\mathbb{L}:(\boldsymbol{\varepsilon}-\gamma\xi\mathbb{K}-(T-T_0)\alpha\mathbb{I}) & \forall(\mathbf{M},t)\in\Omega\times\mathcal{T},\\
\frac{3}{2}\mathrm{d}\boldsymbol{\varepsilon}\mathrm{v}(\boldsymbol{\sigma})-\left(\mathbb{K}+t_k.\dot{\mathbb{K}}\right)(\sigma_{vm}+\alpha)=0 & \forall(\mathbf{M},t)\in\Omega\times\mathcal{T},\\
t_m\ddot{\beta_1}-\left(\beta_1\dot{\beta_1}-\beta_2\dot{\beta_2}\right)\tilde{\mathcal{F}}(\dot{\sigma}_{vm},\pi^f,\beta_1,\beta_2)=0 & \forall(\mathbf{M},t)\in\Omega\times\mathcal{T},\\
\xi=\dfrac{\beta_1^2-\beta_2^2+1}{2} & \forall(\mathbf{M},t)\in\Omega\times\mathcal{T},\\
\beta_1^2+\beta_2^2=1 & \forall(\mathbf{M},t)\in\Omega\times\mathcal{T},\\
\boldsymbol{\sigma}\cdot\mathbf{n}=\mathbf{F_0} & \forall(\mathbf{M},t)\in\Gamma_t\times\mathcal{T},\\
\mathbf{U}=\mathbf{U_0} & \forall(\mathbf{M},t)\in\Gamma_u\times\mathcal{T},\\
T=T_0 & \forall(\mathbf{M},t)\in\Gamma_T\times\mathcal{T},\\
\mathbf{q}\cdot\mathbf{n}=h_0(T-T_0) & \forall(\mathbf{M},t)\in\Gamma_q\times\mathcal{T},\\
\mathbf{U}(\mathbf{M},t_0)=\mathbf{U_i}(\mathbf{M}) & \forall\mathbf{M}\in\Omega,\\
\dot{\mathbf{U}}(\mathbf{M},t_0)=\mathbf{V_i}(\mathbf{M}) & \forall\mathbf{M}\in\Omega,\\
T(\mathbf{M},t_0)=T_i(\mathbf{M}) & \forall\mathbf{M}\in\Omega,
\end{array} \quad (25)$$

with $\tilde{\mathcal{F}}(\dot{\sigma}_{vm},\pi^f,\beta_1,\beta_2)$ given by equation (23). The finally used modeling approach does not introduce any strain rate dependency of the phase transformation behavior as commonly considered for SMA. But the numerical implementation requires adding first order time differential term in equation (22) and second order term in equation (24) to regularize to numerical scheme. Two parameters $t_k$ and $t_m$ are also introduced as time delays in the phase transformation behavior. Physically speaking, these parameters represent the causality constraint preventing 'immediate' phase transformation in the material behavior.

This final system is the one which has been implemented in FE software COMSOL Multiphysics for computing the impact response of a Shape Memory Alloy mechanical system.

## 3. Finite elements model description and numerical implementation

The composition of the SMA used in the numerical applications is $CuAlBe$. Its characteristic phase transformation temperatures measured by electrical resistance evolution are: $M_F^0 = 191\ K$, $M_S^0 = 213\ K$, $A_S^0 = 205\ K$, $A_F^0 = 221\ K$. The material parameters are: $E = 7.5 \times 10^{10}\ Pa$, $\rho = 8129\ kg \cdot m^{-3}$, $\Delta u_0 = 2871.6\ J \cdot m^{-3}$, $\Delta s_0 = 11\ J \cdot m^{-3}$, $\phi_{it} = 100.3\ J \cdot m^{-3}$, $\gamma = 0.0295$, $\alpha = 0.055$, $Cv = 490\ J \cdot kg^{-1}$, $\alpha_0 = 17 \cdot 10^{-6}\ K^{-1}$.

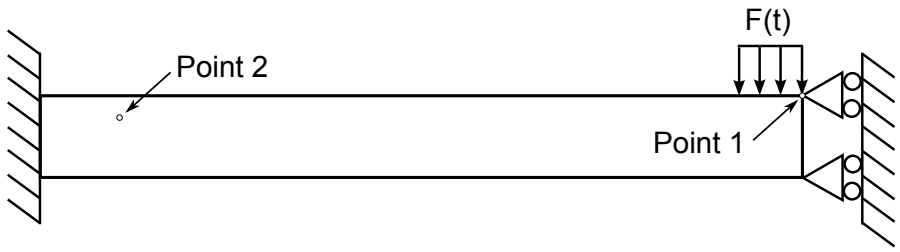


**Figure 3.** 2D-structure: boundary conditions, external forces, observation points 1 and 2

The structure which has been used in the numerical simulations is a 2D plane stress component, shown in figure 3. Its dimensions are 0.5 cm by 10 cm, and the beam is clamped on the border located on $x = 0$ and vertically guided for $x = 0.1\ m$. Two observation points are shown in figure 3. The mesh has 2432 quadratic TRI6 elements, resulting in a total of 18392 degrees of freedom (including components of structural displacement $u = \mathbf{U} \cdot \mathbf{x}$ and $v = \mathbf{U} \cdot \mathbf{y}$, $\beta_1$ and $\beta_2$ values, components of $\mathbb{K}$ and temperature $T$).

Two configurations have been considered in the calculations, the isothermal case and the anisothermal one. The isothermal configuration is evaluated at $T_0 = 293\ K$ and can be interpreted physically as quasistatic in thermal sense. It does not include any temperature effect and corresponds to a basic approach. In order to point out the influence of temperature effects, an anisothermal configuration is also considered. For that case, a constant temperature ($T_0 = 293\,K$) is imposed on the clamped border, and a convective heat transfer with the surrounding environment ($T_0 = 293\,K$), using a heat transfer coefficient value of $5\,W \cdot m^{-2} \cdot K^{-1}$ is imposed on other borders.

The impact force is applied on the upper part of the beam, as shown in figure 3. Its time evolution is shown in figure 4.

The time parameters used for the simulations are $t_m = 1\,ms$ and $t_k = 5\,\mu s$, and a structural damping effect has been used to avoid resonance singularity effects. A very simple Rayleigh model has been chosen using $\alpha_M = 10^{-4} s^{-1}$ and $\beta_K = 10^{-4} s$.

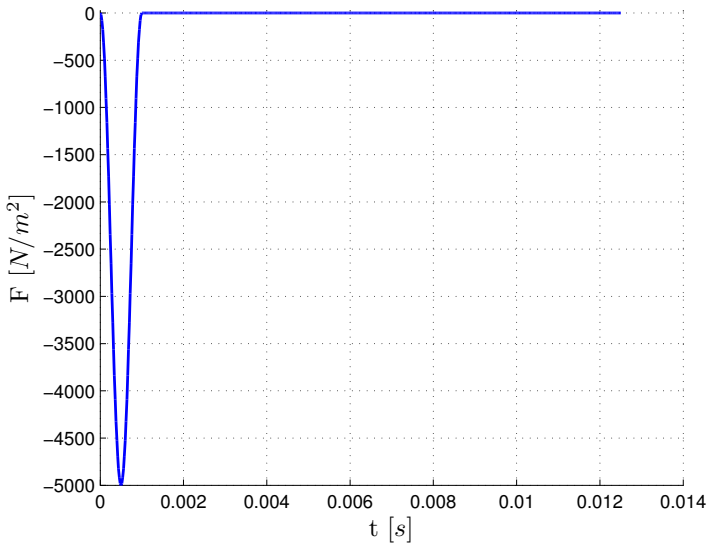


**Figure 4.** Time evolution of the impact force

An implicit time-stepping scheme is used for the time-dependent solver algorithm, based on generalized-$\alpha$ method [23] using a spectral radius of amplification matrix of 0.8. The nonlinear system of equations at each time step is solved using a Newton-Raphson scheme, and the tangent unsymmetric sparse linear system is finally solved using Pardiso solver [24].

## 4. Numerical results

### *4.1. Evaluation of the effect of phase transformation on the displacement amplitude*

As a first observation from the numerical tests, one can note that the phase transformation has a significant effect on the global behavior of the structure, and the thermal effects are also of first importance for pertinent prediction. Figure 5 shows the time evolution of the vertical displacement at point 1 (see figure 3 for the point location), corresponding to three runs. The first one is related to the SMA calculation using isothermal configuration, the second one includes heat equation resolution, and the last one corresponds to a linear equivalent material (linear elastic material with same material properties, without phase change). The first comment about these curves is that one can clearly observe a change in the dynamic properties of the response (lower frequency, higher damping) due to the phase transformations. This point will be detailed in part 4.2. The second comment is that, for the same input force, the maximum total displacement of the structure is higher for the SMA than for the linear material. This is due to the stiffness change of the SMA during phase transformation: as indicated in figure 2, for a given value of stress, the strain is higher on the SMA than on a linear material with equivalent elastic properties. The model has a good physical behavior on this point.

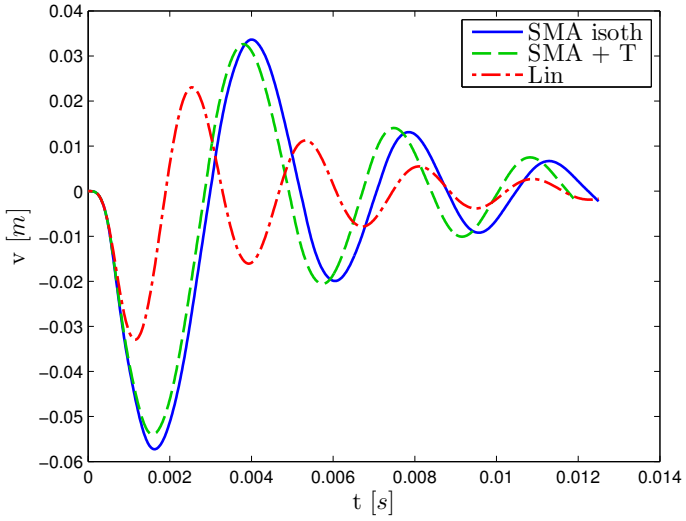


**Figure 5.** Vertical displacement of observation point, comparison of the three calculation configurations

### *4.2. Evaluation of the effect of phase transformation on dynamic properties*

In order to evaluate the effect of phase transformation on dynamic properties, a very simple 1-dof equivalent model can be used to obtain a qualitative information by evaluating the modified frequency and the added damping, with a log-decrement approach. This approach is clearly not efficient enough to characterize the dynamic behavior of the structure because of the strong non linearity of the material. In this context, some dedicated approaches like harmonic balance projection should be used. Nevertheless, the objective of this paper is to present a numerical implementation of the model rather than showing methodologies to use SMA-based structures for dynamic analyses. For that reason, the very basic 1-dof approach allows one to exhibit the physical behavior in a very simple way, using the displacement of point 1 as reference.

For each pseudo-period of the time signal, one can then define a pseudo-frequency and a pseudo-damping ratio. The pseudo-frequency $\tilde{f}$ is:

$$\tilde{f} = \frac{1}{\tilde{t}_2 - \tilde{t}_1}, \tag{26}$$

where $\tilde{t}_1$ and $\tilde{t}_2$ are two (consecutive) times corresponding to sign change of the response. The pseudo-damping ratio $\tilde{\zeta}$ is evaluated using the classical log-decrement formula:

$$\tilde{\zeta} = \frac{1}{\sqrt{1 + 4\frac{\pi^2}{\delta^2}}} \text{ with } \delta = \ln\frac{v(\mathbf{M_1}, t_3)}{v(\mathbf{M_1}, t_4)}, \tag{27}$$

in which $t_3$ and $t_4$ are two (consecutive) times corresponding to local maximum values of the vertical displacement $v$ at point 1.

When the material behavior is linear, it is clear that $\tilde{f}$ and $\tilde{\zeta}$ are constant (they do not depend on the pseudo-period chosen for estimation). Moreover, if the damping is low and only one mode participates to the response, $\tilde{f}$ is equal to the frequency of the responding mode, while $\tilde{\zeta}$ is the damping ratio of the mode.

In the considered situation, both $\tilde{f}$ and $\tilde{\zeta}$ depend on the observation pseudo-period. Figures 6 and 7 compare the linear case to isothermal and anisothermal calculations. In all cases the first "mode" is the main component of the response. The non linear "modes" are changing during time and these curves indicate the trends of their evolution.

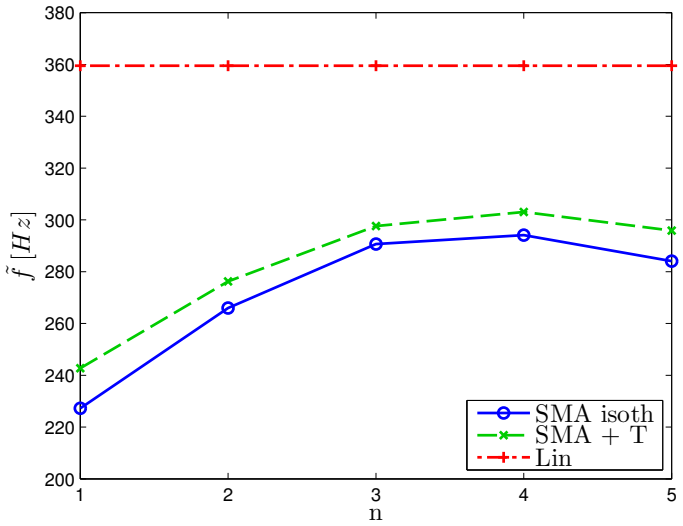


**Figure 6.** Value of pseudo-frequency for each pseudo-period

Figure 6 clearly shows the frequency change : like already seen, the non linear system has a lower rigidity than the linear one, and the corresponding pseudo-oscillating frequency is hence lower. It increases during time evolution because after initial impact, no force is applied on the structure, and a free response is observed. During that movement, the material volume subjected to phase transformation decreases, which induces an increasing apparent frequency. One can note the decrease of pseudo-frequency at step 5, which is not incompatible with the fact that after a finite number of periods, the pseudo-frequency should reach the value of the frequency of the linear model, when no phase transformation still occurs. This depends of course of the material parameters and of the initial phase state. In this case, the very simple approach used to evaluate the pseudo-frequency is clearly not sufficient enough to precisely characterize the non linear behavior. These aspects will be investigated in future dedicated papers.

The pseudo-damping ratio shown in figure 7 illustrates the fact that from an energy point of view, the phase transformations can be seen globally as an increase of losses in the material, which is equivalent to an added damping effect. This added effect exists only when some phase transformations occur: as soon as the thermomechanical system is such that phase transformations can no longer occur, the pseudo-damping ratio is equal to the one of the linear system.

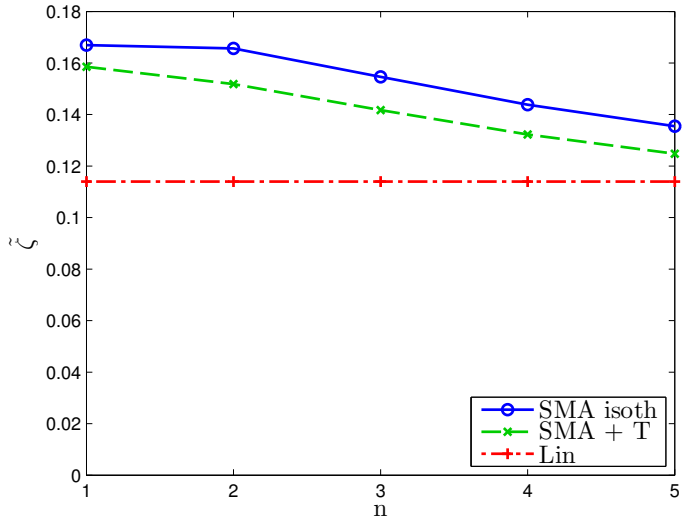


**Figure 7.** Value of pseudo-damping ratio for each pseudo-period

One can finally notice that including temperature effects in the model has non negligible effects: isothermal models should be avoided unless being clearly conscious of the approximation. From a physical point of view, the thermal effects have an inertial effect on the behavior of the structure.

### *4.3. Evolution of phase transformation*

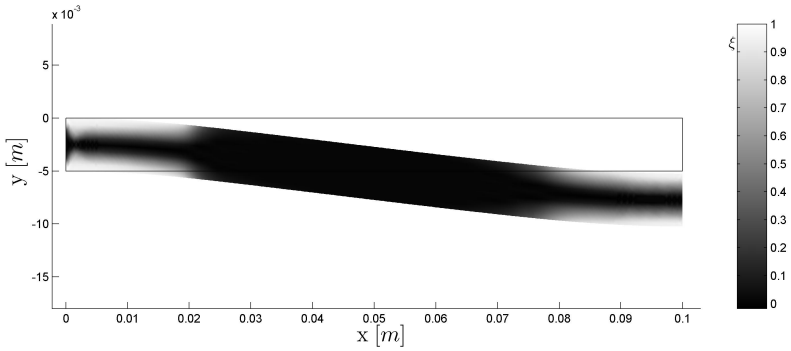


**Figure 8.** Martensite rate distribution at t = 1 ms (end of impact) for the isothermal configuration

On figures 8 and 9, it can clearly be observed that the first mode of the structure is the main component of the time response on both isothermal and anisothermal configurations. The pictures show the spatial displacement of the structure, and the volume fraction of the martensite phase at time corresponding to impact end. The volume fraction of the martensite phase $\xi$ has a large value on areas in which the stress is large, even if the maximum value of $\xi$ at this time is obtained on the right part of the

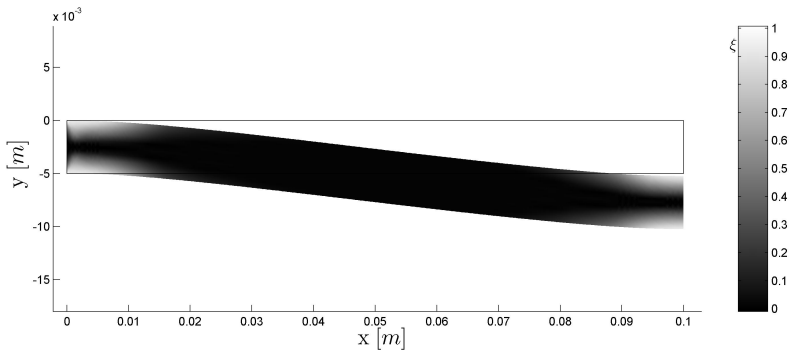


**Figure 9.** Martensite rate distribution at t = 1 ms (end of impact) for the anisothermal configuration

beam, while the maximum Von Mises stress is on the left part, like it will be shown in the next section. The evolution of $\xi$ is governed by the time derivative of the equivalent Von Mises stress, and by the sign of the thermodynamic driving force $\pi^f$. One can observe this physical behavior in figures 10 and 11: while the thermodynamic force is negative, the volume fraction of the martensite phase has a constant zero value. As soon as the driving force becomes positive, $\xi$ increases, until the force becomes negative, because up to 1 ms, the time derivative of the Von Mises stress is always positive. So before 1 ms, each sign change of the thermodynamic force induces an inflection in the curve of the volume fraction of the martensite phase.

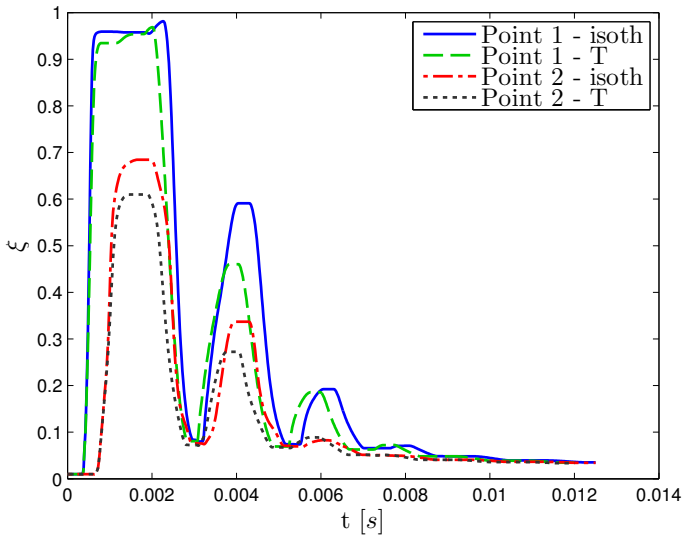


**Figure 10.** Time evolution of volume fraction of the martensite phase at observation points for both isothermal and anisothermal configurations

Once again the inertial effects associated to phase transformation can clearly be seen by comparing isothermal and anisothermal configurations.

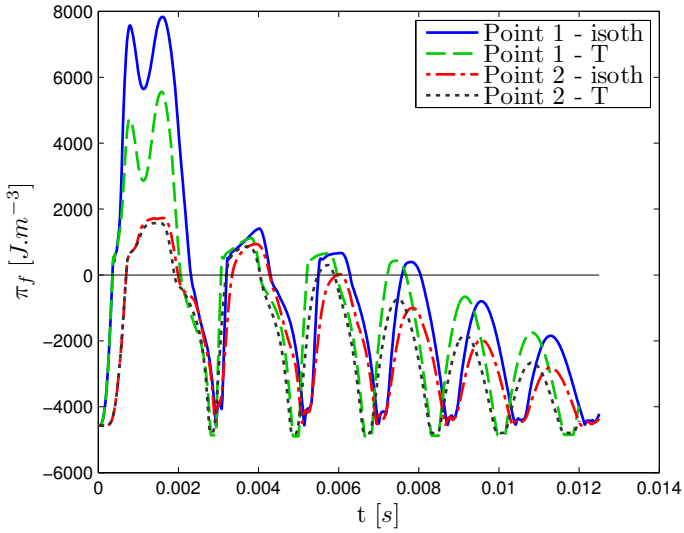


**Figure 11.** Time evolution of driving force $\pi^f$ for both isothermal and anisothermal configurations

### *4.4. Evaluation of the effect of phase transformation on temperature*

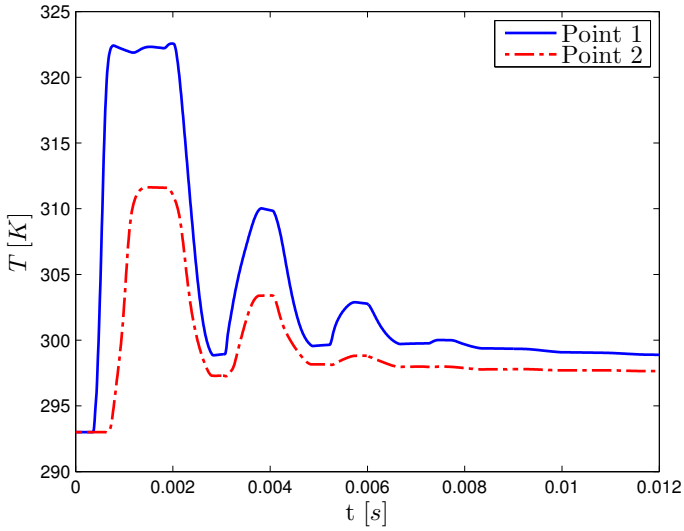


**Figure 12.** Time evolution of temperature for anisothermal configuration

Figure 12 shows the time evolution of temperature for the anisothermal calculation. One can observe the temperature changes due to phase transformation. In the considered case, a quasi-instantaneous shift of 30 $K$ has been observed at point 1. This particular consideration will be of first interest in next works associated to experimental validation of the model: if some variables like $\xi$ cannot be measured, the temperature field $T$ on the border of the structure can be evaluated using an infrared camera. For that particular objective of model validation, being able to include thermal effects in the calculation is

of first importance.

### *4.5. Evaluation of the effect of phase transformation on the equivalent Von Mises stress*

The time evolution of the Von Mises stress is of particular importance in the model, since its time derivative is governing the volume fraction of the martensite phase evolution. A good evaluation of this stress is necessary to obtain a coherent volume fraction of the martensite phase time evolution. In figures 13 and 14, the spatial repartition of the Von Mises stress is shown at $t$=1 ms, and one can observe that its distribution is physical: a maximum value on the upper and lower bounds of the beam, close to the clamped boundary conditions. In this particular case, the stresses have been correctly evaluated, even for this particular zone thanks to the small size of elements, but it could be possible that this displacement formulation for the mechanical problem would not be sufficient to evaluate the stresses. In this case a mixed formulation could possibly be more efficient.

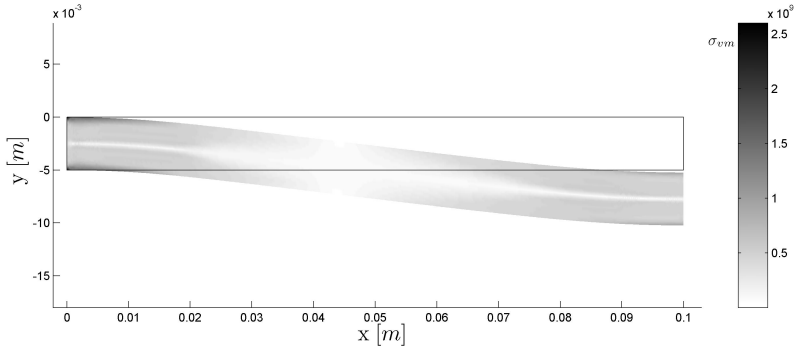


**Figure 13.** Spatial repartition of Von Mises equivalent stress at $t$=1 ms for isothermal configuration

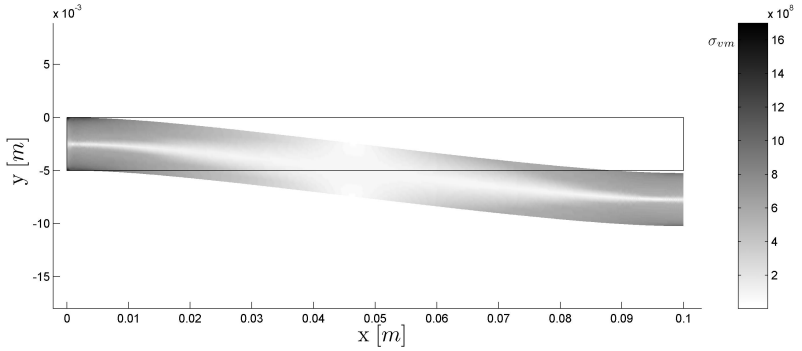


**Figure 14.** Spatial repartition of Von Mises equivalent stress at $t$=1 ms for anisothermal configuration

The figure 15 shows the time evolution of Von Mises equivalent stress on observation points, for the SMA calculation and for the linear model. One can observe that the

maximum stress level has been obtained for the linear model, while the energy required for phase transformation of the SMA induces lower values of stress.

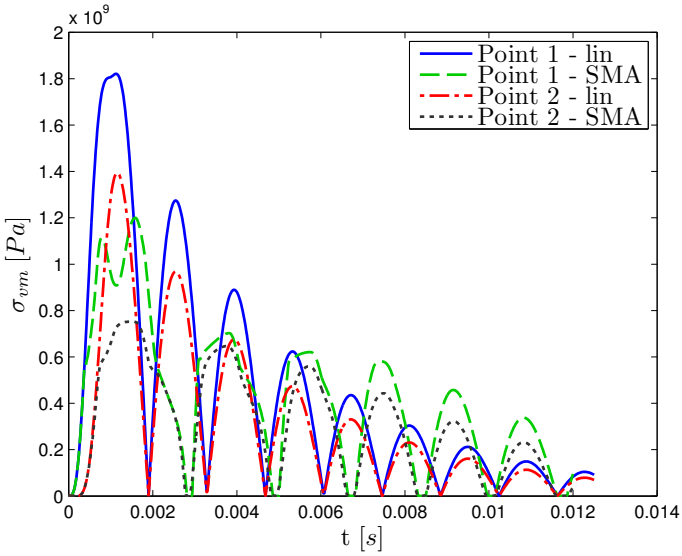


**Figure 15.** Time evolution of Von Mises equivalent stress at observation points for linear equivalent model and anisothermal configurations

Figure 16 compares time evolutions of Von Mises equivalent stresses at observation points for both isothermal and anisothermal configurations. Stresses are of the same order of magnitude, and the inertial effect of temperature can be observed one more time.

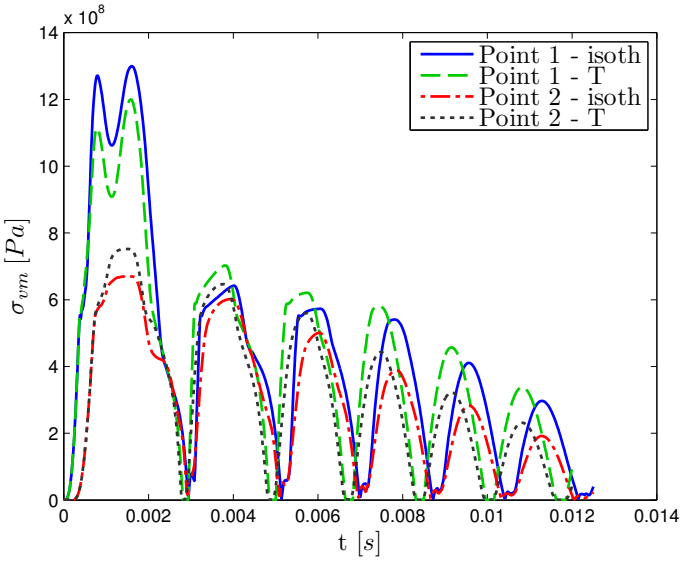


**Figure 16.** Time evolution of Von Mises equivalent stress at observation points for isothermal and anisothermal configurations

### *4.6. Evaluation of the effect of phase transformation on Head Injury Criterion*

When people are dealing with impact evaluation, a criterion that is commonly used it the Head Injury Criterion (HIC). This indicator allows one to compare for example the efficiency of shock absorber devices. It is used in particular in some international normative procedures. The expression of the HIC is:

$$HIC = \max_{t_1,t_2} \left[ (t_2 - t_1) \left( \frac{1}{t_2 - t_1} \int_{t_1}^{t_2} ||\ddot{\mathbf{U}}|| dt \right)^{2.5} \right], \tag{28}$$

in which $t_1$ and $t_2$ are time steps in the interval of interest. The value of HIC for the three configurations of interest are respectively:

- $15.2 \times 10^{-3}$ for the linear case,
- $9.3 \times 10^{-3}$ for the isothermal case,
- $1.9 \times 10^{-3}$ for the anisothermal case.

These values can be understood by looking at the value of HIC when time $t_1$ increases: the corresponding time evolutions are given in figure 17.

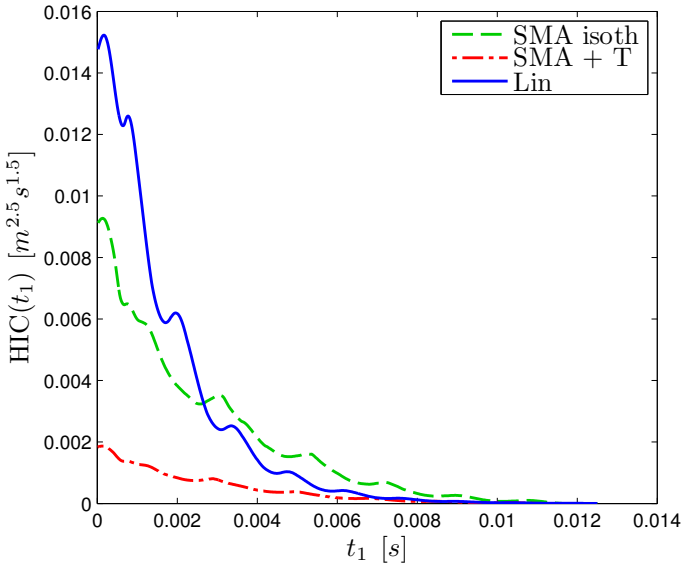


**Figure 17.** HIC evolution with initial time integration $t_1$, comparison of the three configurations

One can clearly see the positive effect of the SMA device on the criterion. An interesting thing is that including thermal effects induces a reduction of HIC value. Demonstrating the effectiveness of SMA for shock absorption is not the aim of this paper, but one can observe that for the considered structure, with a given impact force, the SMA allows a large reduction of impact indicator compared to an equivalent linear system. Nevertheless, the strong non linearities of the material behavior, associated to the fact that no plasticity effects have been considered should induce people to take

care about hurried conclusions. Some complementary analyses are necessary to have a pertinent opinion on the efficiency of SMA devices for shock absorption. Nevertheless, these first results are clearly encouraging ourselves to investigate this way.

## 5. Conclusions

In this paper a numerical implementation of a shape memory alloy model in the context of structural transient response to impact load using the finite elements method has been proposed. The initial *RL* model has been adapted in order to take into account the specific numerical difficulties inherent to this kind of calculation. The model includes full thermomechanical coupling, and numerical tests have been presented in order to show the effects of the SMA material (compared with an equivalent linear model), and also the effects of the heat exchanges in the problem. The numerical behavior of the model has not exhibited any unphysical phenomenon.

As far as the model itself is concerned, the next improvement will be the inclusion of the tension/compression asymmetry which has not been considered here. This model will then be compared with experimental data, in order to fully validate the approach. After that step, one will be able to describe properly the non linear dynamical SMA-based structure using dedicated methods, while the final goal will be to include plasticity effects in the model in order to provide a full model for crash simulation using SMA devices.

## Acknowledgements

The authors would like to thank the french research and innovation program PREDIT for the financial support of a part of this work.

## References

[1] B. Raniecki, C. Lexcellent, and K. Tanaka. Thermodynamic models of pseudoelastic behaviour of shape memory alloys. *Archives of Mechanics-Archiwum Mechaniki Stosowanej*, 44(3):261–284, 1992.

[2] B. Raniecki and C. Lexcellent. Rl- models of pseudoelasticity and their specification for some shape memory solids. *European Journal of Mechanics A/Solids*, 13(1):21–50, 1994.

[3] B. Raniecki and C. Lexcellent. Thermodynamics of isotropic pseudoelasticity in shape memory alloys. *European Journal of Mechanics A/Solids*, 17, 1998.

[4] T. Atanacković and M. Achenbach. Moment-curvature relations for a pseudoelastic beam. *Continuum Mechanics and Thermodynamics*, 1(1):73–80, 1989.

[5] J. Rejzner, C. Lexcellent, and B. Raniecki. Pseudoelastic behaviour of shape memory alloy beams under pure bending: experiments and modelling. *International Journal of Mechanical Sciences*, 44(4):665–686, 2002.

[6] A. Sadjadpour and K. Bhattacharya. A micromechanics inspired constitutive model for shape-memory alloys: the one-dimensional case. *Smart Materials and Structures*, 16(1):51, 2007.

[7] F. Auricchio, R.L. Taylor, and J. Lubliner. Shape-memory alloys: macromodelling and numerical simulations of the superelastic behavior. *Computer Methods in Applied Mechanics and Engineering*, 146(3-4):281–312, 1997.

[8] P. Sittner, Y. Hara, and M. Tokuda. Experimental study on the thermoelastic martensitic transformation in shape memory alloy polycrystal induced by combined external forces. *Metallurgical and Materials Transactions A*, 26(11):2923–2935, 1995.

[9] B. Halphen and Q.S. Nguyen. Plastic and viscoplastic materials with generalized potential. *Mechanics Research Communication*, 1:43–47, 1974.

[10] Z. Moumni, W. Zaki, and Q.S. Nguyen. Theoretical and numerical modeling of solid–solid phase change: Application to the description of the thermomechanical behavior of shape memory alloys. *International Journal of Plasticity*, 24(4):614–645, 2008.

[11] J.C. Escobar and R.J. Clifton. On pressure-shear plate impact for studying the kinetics of stress-induced phase transformations. *Materials Science and Engineering: A*, 170(1-2):125–142, 1993.

[12] R. Abeyaratne and J.K. Knowles. On the kinetics of an austenite - martensite phase transformation induced by impact in a cu al ni shape-memory alloy. *Acta Materialia*, 45(4):1671–1683, 1997.

[13] R. Abeyaratne and J.K. Knowles. *Evolution of phase transitions: a continuum theory*. Cambridge University Press, 2006.

[14] K.A. Tsoi, R. Stalmans, J. Schrooten, M. Wevers, and Y.W. Mai. Impact damage behaviour of shape memory alloy composites. *Materials Science & Engineering A*, 342(1-2):207–215, 2003.

[15] J. Tandler, E. Zimmerman, V. Muntean, B. Seipel, T. Koch, D. Willersinn, M. Grinberg, C. Mayer, and M. Diez. A new pre-crash system for side impact protection. *International Journal of Crashworthiness*, 13(6):679–692, 2008.

[16] P. Qiao, M. Yang, and Bobaru; F. Impact mechanics and high-energy absorbing materials: Review. *Journal of Aerospace Engineering*, 2(4):235–248, 2008.

[17] Y.C. Chen and D.C. Lagoudas. Impact induced phase transformation in shape memory alloys. *Journal of the Mechanics and Physics of Solids*, 48(2):275–300, 2000.

[18] F. Thiebaud, C. Lexcellent, M. Collet, and E. Foltête. Implementation of a model taking into account the asymmetry between tension and compression, the temperature effects in a finite element code for shape memory alloys structures calculations. *Computational Materials Science*, 41(2):208–221, 2007.

[19] S.Y. Yang, J. Escobar, and R.J. Clifton. Computational modeling of stress-wave-induced martensitic phase transformations in niti. *Mathematics and Mechanics of Solids*, 14(1-2):220–257, 2009.

[20] F. Auricchio and A. Reali. Shape memory alloys: material modeling and device finite element simulations. *Materials Science Forum*, 583:257–275, 2008.

[21] A. Airoldi, G. Corsi and G. Riva. Step-wise martensite to austenite reversible transformation stimulated by temperature or stress: a comparison in niti alloys. *Materials science & engineering. A, Structural materials: properties, microstructure and processing*, 241(1-2):233–240, 1998.

[22] K. Tanaka, F. Nishimura, T. Hayashi, H. Tobushi, and C. Lexcellent. Phenomenological analysis on subloops and cyclic behavior in shape memory alloys under mechanical and/or thermal loads. *Mechanics of Materials*, 19(4):281–292, 1995.

[23] J. Chung and G.M. Hulbert. A time integration algorithm for structural dynamics with improved numerical dissipation: the generalized-$\alpha$ method. *ASME Journal of Applied Mechanics*, 60:371, 1993.

[24] O. Schenk and K. Gärtner. Solving unsymmetric sparse systems of linear equations with pardiso. *Future Generation Computer Systems*, 20(3):475–487, 2004.